

Microstructure and magnetic properties of FePt and Fe/FePt polycrystalline films with high coercivity

Y. K. Takahashi^{a)}

National Institute for Materials Science, 1-2-1 Sengen, Tsukuba 305-0047, Japan

T. O. Seki

Graduate School of Pure and Applied Science, University of Tsukuba, Tsukuba 305-8577, Japan

K. Hono

National Institute for Materials Science, 1-2-1 Sengen, Tsukuba 305-0047, Japan

and Graduate School of Pure and Applied Science, University of Tsukuba, Tsukuba 305-8577, Japan

T. Shima and K. Takanashi

Institute for Materials Research, Tohoku University, Sendai 980-8577, Japan

(Received 29 December 2003; accepted 2 April 2004)

We have investigated the microstructure and the magnetic properties of FePt and Fe/FePt polycrystalline thin films with high coercivity. The $L1_0$ FePt particulate film deposited on a heated amorphous SiO_2 substrate showed a large coercivity (H_c) as high as 23 kOe. Contrary to an epitaxially grown single crystal FePt film, the H_c did not show a drastic decrease when the film morphology changed from particulate to continuous. The polycrystalline film with a thickness of 100 nm exhibited a coercivity of 13 kOe in spite of its simple processing route. This high coercivity is attributed to the magnetic domain pinning at the grain boundaries. By depositing Fe layers on the particulate FePt films, an increase of remanence and energy product was observed as a result of the exchange coupling of the Fe and FePt layers. © 2004 American Institute of Physics.

[DOI: 10.1063/1.1756688]

I. INTRODUCTION

Since Coehoon *et al.*¹ reported the experimental results of the exchange coupled nanocomposite magnet, many investigations have been carried out to achieve high energy products from the nanocomposite microstructures comprised of soft and hard magnetic phases.²⁻⁷ Fe/FePt nanocomposites are promising candidates to achieve high energy product due to the large magnetocrystalline anisotropy ($\sim 7 \times 10^7$ erg/cc)⁸ of the $L1_0$ FePt phase and the high saturation magnetization of the α -Fe phase. Sabiryayov and Jaswal⁷ predicted an energy product of 90 MGOe from a FePt/Fe nanocomposite by the first principle calculation, and Liu *et al.*⁶ succeeded in fabricating a FePt/Fe₃Pt nanocomposite thin film with an energy product of 52.8 MGOe by rapidly annealing Fe/Pt multilayer thin films.

FePt films are expected to show very high coercivity because of the high magnetocrystalline anisotropy of the $L1_0$ FePt phase. The theoretical limit of the coercivity predicted from the anisotropy constant is about 120 kOe. However, continuous FePt thin films produced by simple processing methods such as sputtering and vacuum vapor deposition methods did not show high coercivities.^{9,10} Watanabe and Homma¹¹ reported a high coercivity for the FePt thin films deposited on a Pt underlayer, and it was later shown that this high coercivity was linked with the multitwins that were introduced from the Pt/FePt interfaces.¹² Ide *et al.*¹³ reported a

large coercivity of 48 kOe in very thin island-like grown films, but its coercivity decreases when the film thickness increases. Shima *et al.*¹⁴ and Okamoto *et al.*¹⁵ also reported a very large coercivity exceeding 40 kOe for particulate films epitaxially grown on heated MgO single crystal substrates. However, the coercivity drops drastically to about 2 kOe when the film becomes continuous after growing to a thickness of more than 40 nm, because there are few domain wall pinning sites in the single crystalline film. To achieve high coercivity in continuous FePt thin films, an introduction of a domain wall pinning sites is necessary. Hence, the polycrystalline films should be more suitable to achieve high coercivity in continuous films.^{16,17}

In this work, we have fabricated FePt polycrystalline films with high coercivity on a thermally oxidized Si substrates. Furthermore, we have investigated the possibility of enhancing the energy product by producing Fe/FePt nanocomposite thin films. We discuss the coercivity mechanism of the FePt thin films by comparing the microstructures of the polycrystalline FePt thin films with those of the single crystal thin films fabricated on MgO substrates.¹⁴

II. EXPERIMENT

FePt films with various thicknesses ranging from 10 to 100 nm were prepared by co-sputtering high purity (99.99%) Fe and Pt targets on heated substrates using a multiple dc-sputtering system. Thermally oxidized Si wafers were used as substrates, which were coated with an amorphous SiO_2 layer. The substrates were heated at 700 °C on a rotating table during film deposition. The base pressure of the system

^{a)} Author to whom correspondence should be addressed; electronic mail: takahashi.yukiko@nims.go.jp

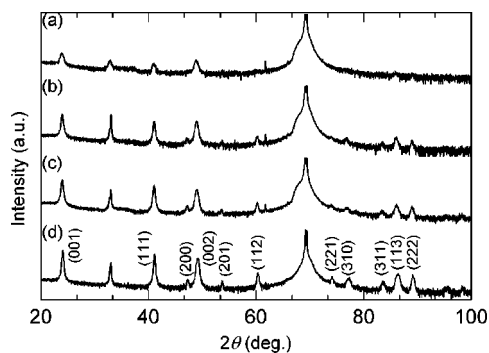


FIG. 1. XRD patterns for various thicknesses of FePt films: 10 nm (a), 30 nm (b), 38 nm (c), and 100 nm (d).

was 6.0×10^{-7} Pa, and a high-purity argon of 0.1 Pa was flown during sputtering. The growth rate of FePt was controlled to 0.10 nm/s and the nominal thickness was evaluated based on the sputtering time. To produce Fe/FePt nanocomposites, Fe layers of 20%, 40%, and 60% of FePt thickness were deposited on the FePt film at room temperature. The film structures were characterized by x-ray diffraction (XRD) and transmission electron microscopy (TEM). The compositions of the FePt estimated by energy dispersive x-ray spectroscopy were about $\text{Fe}_{50}\text{Pt}_{50}$ for all the films. The magnetic properties of the films were examined by a superconducting quantum interference device magnetometer.

III. RESULTS

A. FePt film

Figure 1 shows x-ray diffraction patterns for the FePt films with various thicknesses, $t = 10$ nm (a), 30 nm (b), 38 nm (c), and 100 nm (d). Superlattice diffraction lines of (001) and (112) are clearly observed around $2\theta = 24^\circ$ and 60° , respectively. All the films are ordered to the $L1_0$ structure in the as-deposited state. The other unlabeled sharp

peaks are due to the Si substrate. The relative integrated intensities of (001) and (111) indicates that all the films have a weak preferred orientation to [001] in the perpendicular direction to the film plane.

Figure 2 shows TEM bright field images of the FePt films with various thicknesses. The inset selected area electron diffraction (SAED) patterns show that all the films are in the $L1_0$ ordered state, because the superlattice diffraction rings of (001) and (110) are clearly observed as indicated by the arrows. The average particle size of the 10 nm thick film is about 50 nm. The FePt particles are completely isolated with each other. With increasing the film thickness, the average particle size increases. The films that are thicker than 60 nm have an interconnected network structure. This morphological change is the same as that observed in the FePt film deposited on a MgO (001) single crystal substrate.¹⁴ Twins are commonly observed in the particles as indicated by the arrows. Figure 3 shows a typical [011] nanobeam diffraction pattern obtained from one of the grains that contain a twin. The twin was identified as the $(11\bar{1})$ twin, so this is different from the transformation twins that form when fcc disordered phase transform to the $L1_0$ tetragonal lattice.¹⁸ Hence, these twins are believed to be growth twins which commonly occur in the fcc crystals during growth by various thin film processing. The $\{111\}$ twins in the $L1_0$ ordered FePt thin films were also reported by Hong *et al.*¹⁹

Figure 4 shows magnetization curves of the FePt films with $t = 10$ nm (a), 20 nm (b), 30 nm (c), 38 nm (d), 60 nm (e), and 100 nm (f). The filled and open circles show the magnetization curves in the perpendicular and in-plane directions to the film, respectively. The magnetization curves are not corrected with the demagnetization factors. The films that are thicker than 30 nm show weak perpendicular anisotropy due to the development of the [001] preferred orientation during the film growth. Because of the high magneto-crystalline anisotropy of the isolated particles, the

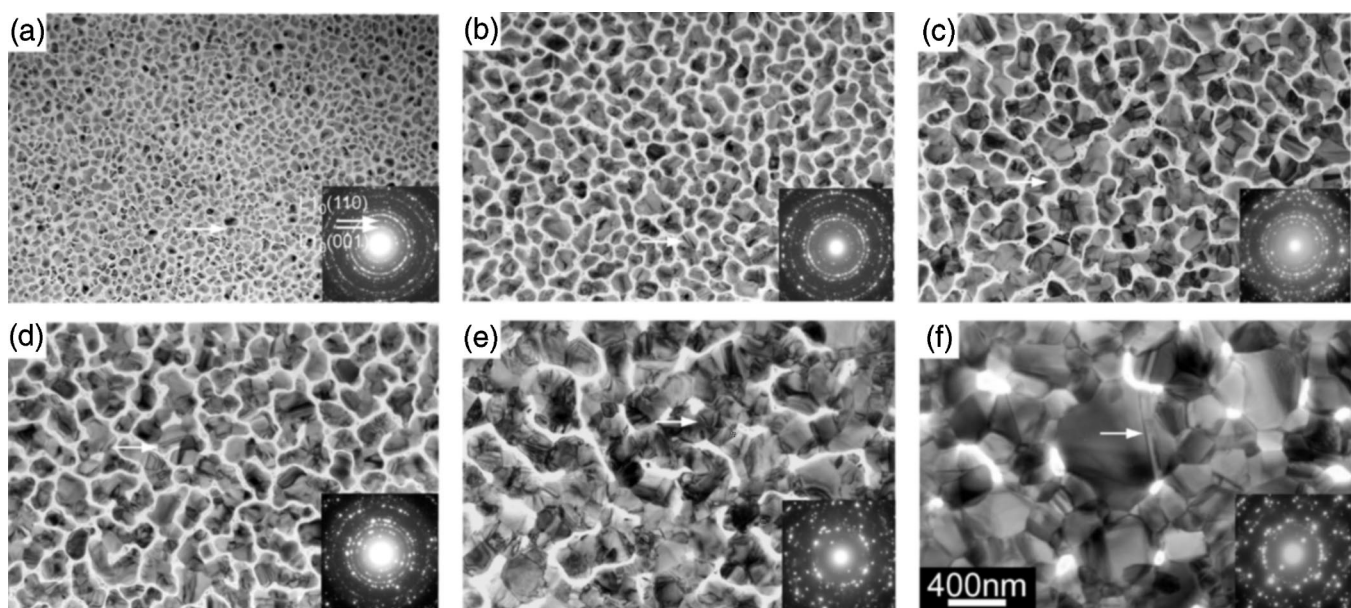


FIG. 2. TEM images and SAED patterns for various thicknesses of FePt films: 10 nm (a), 20 nm (b), 30 nm (c), 38 nm (d), 60 nm (e), and 100 nm (f).

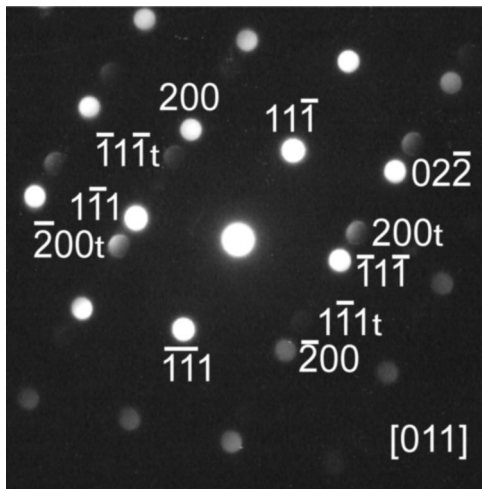


FIG. 3. [011] nanobeam diffraction pattern obtained from one of the grains that contains a twin.

magnetization curves of the films with $t=10$ and 20 nm do not saturate even at a magnetic field of 55 kOe. A large coercivity (H_c) of about 23 kOe was obtained from the 10 nm thick film. H_c gradually decreases with increasing the film thickness, but still shows a high H_c of about 13 kOe at $t=100$ nm. The initial magnetization curves for the 10 nm and 20 nm thick films are characteristic of the rotation magnetization, because large magnetic field is required to magnetize the particles. On the other hand, those for 60 and 100 nm thick films are characteristic of the domain wall displacement because the initial magnetization curve indicate that the

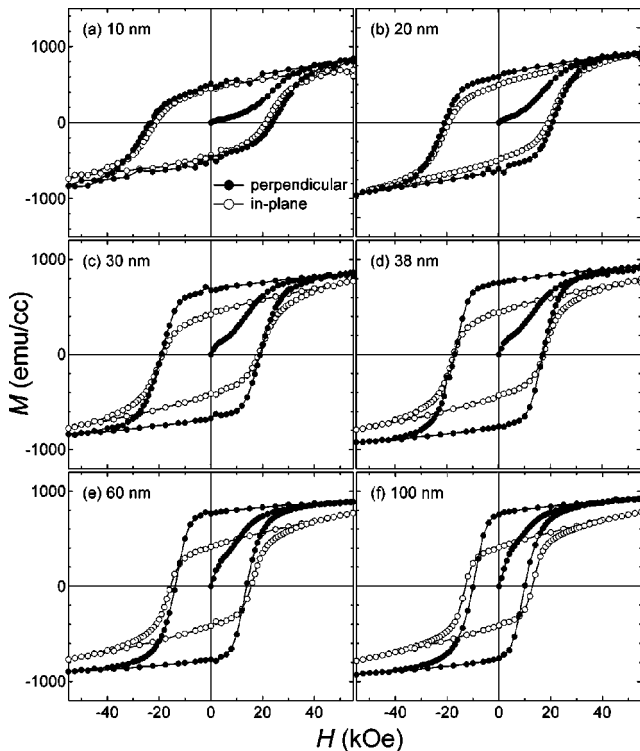


FIG. 4. Magnetization curves with initial magnetization curve of various thicknesses of FePt films. Filled and opened circles show the magnetization curves in the perpendicular and in-plane direction to the film, respectively.

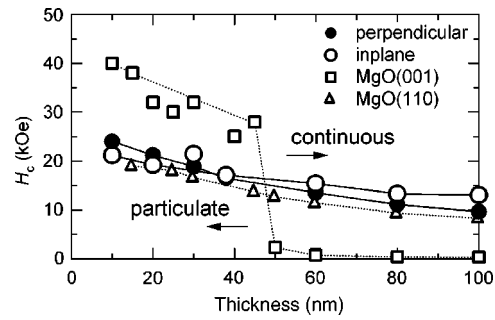


FIG. 5. Change of H_c as a function of the film thickness.

magnetization progress easily at the low magnetic field. Figure 5 shows the change of H_c as a function of the film thickness. The H_c of the FePt films deposited on MgO (001)¹⁴ and MgO (110)²⁰ single crystal substrates are also shown in the same figure. With increasing film thickness, the H_c for the films deposited on the SiO_2 substrates decreases gradually, while the H_c for the single crystal films deposited on MgO (001) substrates shows a drastic decrease when the film thickness is more than 40 nm. The gradual decrease of H_c in the polycrystalline film as a function of film thickness is similar to that observed in the FePt film deposited on a MgO (110) substrate.²⁰

B. Fe/FePt film

To obtain a higher energy product by making a nanocomposite with a soft phase, Fe was deposited on 10 and 38 nm thick FePt particulate films. Figures 6 and 7 show the in-plane and cross section TEM bright field images of: (a) FePt 10 nm film, (b) Fe 2 nm/FePt 10 nm, (c) Fe 4 nm/FePt 10 nm, and (d) Fe 6 nm/FePt 10 nm bilayer films. The Fe (110) diffraction ring is clearly observed in Fig. 6(d). The plan-view image shows that the film morphology is particu-

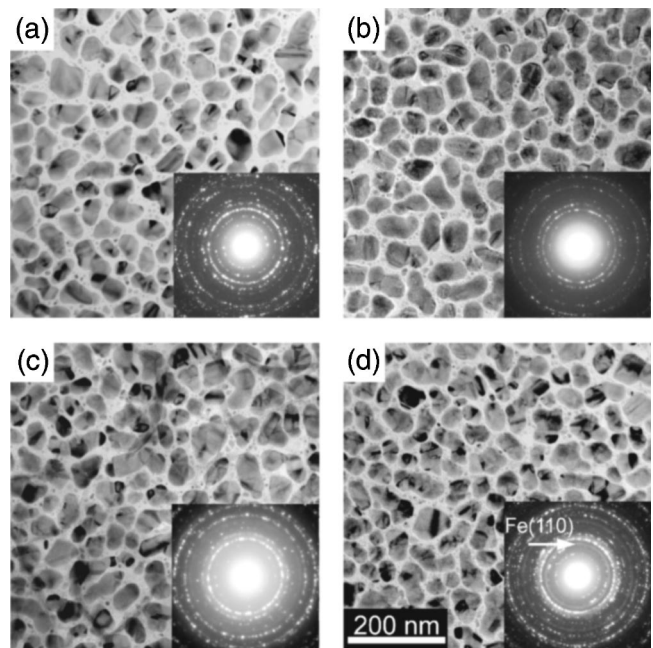


FIG. 6. TEM images and SAED patterns of Fe/FePt 10 nm bilayer films.

ties are summarized in Table II. By depositing the Fe layer, the H_c decreases drastically. On the other hand, the residual magnetization, M_r , increases with the Fe thickness. As a result, the energy product increases with the Fe thickness. The highest energy product is about 16.9 MGOe.

late for all the bilayer films. The cross-sectional image shows that the FePt particles had relatively flat surface with nearly the same thickness. The height of the particles increases after the deposition of the Fe layers, and their shape becomes round as the thickness of Fe increases. Figure 8 shows the magnetization curves of (a) FePt 10 nm film, (b) Fe 2 nm/FePt 10 nm, (c) Fe 4 nm/FePt 10 nm, and (d) Fe 6 nm/FePt 10 nm bilayer films. The magnetization curves are corrected with the demagnetization factors as shown in Table I from the average particle size observed from Figs. 6 and 7, assuming the ellipsoidal shape of particles. Their magnetic proper-

TABLE II. Magnetic properties of Fe/FePt 10 nm bilayer films.

Fe (nm)	$H_{c\perp}$ (kOe)	$H_{c\parallel}$ (kOe)	$M_{r\perp}$ (emu/cc)	$M_{r\parallel}$ (emu/cc)	$(BH)_{\max\perp}$ (MGOe)	$(BH)_{\max\parallel}$ (MGOe)
0	22.9	21.1	475	450	12.4	7.6
2	19.2	18.1	585	438	13.7	6.6
4	12.1	9.4	680	625	13.8	11.0
6	9.2	5.5	800	890	15.3	16.9

phases, viz., Fe soft magnetic phase and $L1_0$ FePt hard magnetic phase. The in-plane magnetization curve of the films whose Fe layer is thicker than 15.2 nm shows decoupled two magnetic phases. One is due to the Fe soft magnetic phase which accounts for the decrease in magnetization at around 0 Oe. The other is due to the $L1_0$ FePt hard magnetic phase which accounts for the decrease in magnetization in the high magnetic field region.

IV. DISCUSSION

High coercive FePt thin films are fabricated on heated SiO_2 substrates. While H_c of the film deposited on a MgO (001) substrate shows a drastic decrease by 1 order of magnitude when the morphology of the film changes from particulate to the continuous structure,¹⁴ the change of the morphology of the films deposited on the SiO_2 substrate does not cause the drastic decrease in coercivity. The FePt films on SiO_2 are polycrystal and those on MgO (001) are single crystal.¹⁴ The large H_c of the polycrystalline continuous films are caused by the strong pinning of the magnetic domain walls at the grain boundaries and the twins within the grains. Since the K_u of the $L1_0$ ordered FePt is very large, misorientation of the easy axis at the grain boundary and

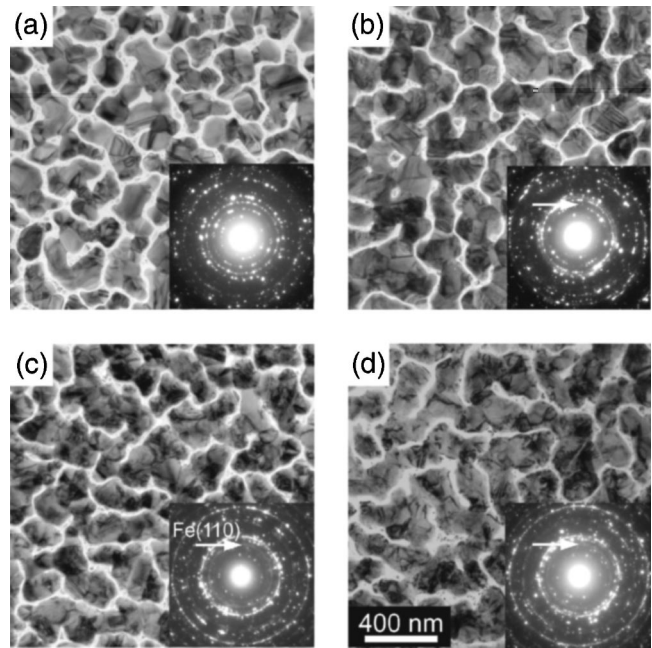


FIG. 9. TEM images and SAED patterns of Fe/FePt 38 nm bilayer films.

twins will act as domain wall pinning sites.²¹ On the other hand, since single crystalline FePt continuous films have neither grain boundaries nor twins, no pinning sites for magnetic domain motion are expected. The gradual decrease in coercivity will be explained by the continuous coarsening of the grain size as the films are grown on the heated substrates, by which the number of domain wall pinning sites decreases. The change of the magnetic domain reversal mechanism from the rotation mode to the nucleation mode will also ex-

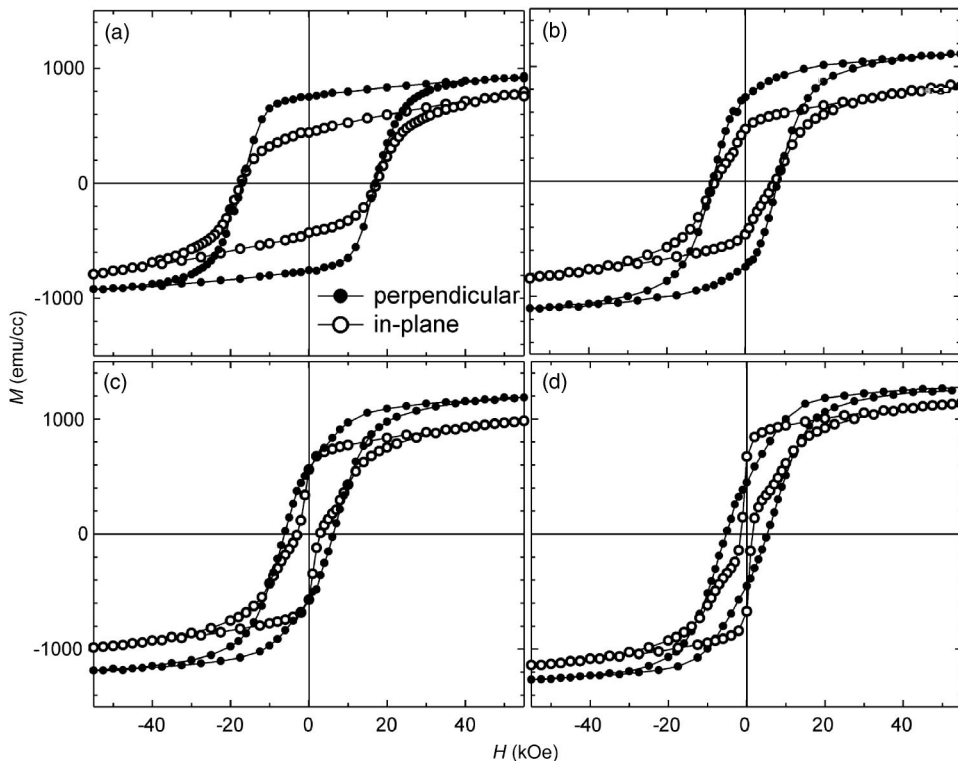


FIG. 10. Magnetization curves of Fe/FePt 38 nm bilayer films. The magnetization curves are not corrected by the demagnetization factors.

plain the gradual decrease of the coercivity. If grain size can be kept small, higher coercivity may be achieved even in the thick films.

The critical size of a single domain particle with a flat ellipsoidal shape, d , is given by²²

$$d = \frac{24\sqrt{AK_u}}{NM_s^2}, \quad (1)$$

where A is the exchange stiffness constant, K_u is the uniaxial anisotropy constant, N is the demagnetization factor, and M_s is the saturation magnetization. For $L1_0$ FePt, $A = 1 \times 10^{-6}$ erg/cm,²³ $K_u = 7 \times 10^7$ erg/cc,⁸ and $M_s = 1150$ emu/cc.⁸ In the 10 nm-thick film, N_{\perp} is about 7.81. Substituting the demagnetization factor for Eq. (1), the critical particles size of the single domain is estimated to be about 200 nm. In the 10 and 20 nm thick films, the particle size is smaller than the single domain size. Hence, the initial magnetization curves observed in Figs. 4(a) and 4(b) are explained by the rotation mechanism. In 60 and 100 nm thick films [Figs. 4(e) and 4(f)], the morphology changes to a continuous structure. The initial magnetization curve is characterized as the nucleation type, although there are twins and grain boundaries which can act as pinning sites for domain wall motion. This is because each of the grains can be easily magnetized by the domain wall displacement from a multiple domain to a single domain state, because there are few pinning sites within the grains. Although the twins within the grains can act as pinning sites, the number of twins also decreases with the increase of the film thickness.

In the 30 and 38 nm thick films [Figs. 4(c) and 4(d)], the magnetization increases rapidly at a low magnetic field and increases slowly at a high magnetic field. From the TEM bright field images, the films consist of isolated polycrystalline particles. The initial magnetization at the low magnetic field region is due to the nucleation-type magnetization within the crystal grains. At this stage, the orientation of the magnetization within the grains will be aligned to the c axis of each grain by domain wall displacement within the grains. The second increase of the magnetization above 3 kOe is attributed to the rotation magnetization of randomly oriented

- (1) The film morphology changes from a particulate structure to a continuous structure with increasing film thickness.
- (2) The 10 nm thick FePt film shows a high H_c such as 23 kOe. The H_c decreases gradually with an increase in the film thickness, not showing a drastic decrease like that in the single crystalline FePt films deposited on a MgO (001) single crystal substrate. High coercivity in the polycrystalline film is due to the magnetic domain pinning at the grain boundaries and the twins in the grains.
- (3) Exchange coupled Fe/FePt bilayer thin films showed improved energy products of $(BH)_{\max} \sim 16.9$ MGOe.

ACKNOWLEDGMENTS

This work was partly supported by the Special Coordination Funds for Promoting Science and Technology on "Nanohetero Metallic Materials" from the Ministry of Education, Culture, Sports, Science and Technology. One of the authors (Y.K.T.) acknowledges the Japan Science Promotion Society for a JSPS fellowship.

- ¹R. Coehoorn, D. B. de Mooij, and C. de Waard, *J. Magn. Magn. Mater.* **80**, 101 (1989).
- ²E. F. Kneller and R. Hawig, *IEEE Trans. Magn.* **27**, 3588 (1991).
- ³R. Fischer, T. Schrefl, H. Kronmüller, and J. Filder, *J. Magn. Magn. Mater.* **153**, 35 (1996).
- ⁴S. Hirohara, H. Kanekiyo, and M. Uehara, *J. Appl. Phys.* **73**, 6488 (1993).
- ⁵D. C. Crew, J. Kim, L. H. Lewis, and K. Barmak, *J. Magn. Magn. Mater.* **233**, 257 (2001).

- ⁶J. P. Liu, C. P. Luo, Y. Liu, and D. J. Sellmyer, *Appl. Phys. Lett.* **72**, 483 (1998).
- ⁷R. F. Sabirianov and S. S. Jaswal, *J. Magn. Magn. Mater.* **177–181**, 989 (1998).
- ⁸O. A. Ivanov, L. V. Solina, V. A. Demshina, and L. M. Maget, *Phys. Met. Metallogr.* **35**, 81 (1973).
- ⁹T. Shima, T. Moriguchi, S. Mitani, and K. Takahashi, *Appl. Phys. Lett.* **80**, 288 (2001).
- ¹⁰Y. K. Takahashi, M. Ohnuma, and K. Hono, *Jpn. J. Appl. Phys., Part 2* **40**, L1367 (2001).
- ¹¹M. Watanabe and M. Homma, *Jpn. J. Appl. Phys., Part 1* **35**, 1264 (1996).
- ¹²M. H. Hong, K. Hono, and M. Watanabe, *J. Appl. Phys.* **84**, 4403 (1998).
- ¹³Y. Ide, T. Goto, K. Kikuchi, K. Watanabe, J. Onagawa, H. Yoshida, and J. M. Cadogan, *J. Magn. Magn. Mater.* **177–181**, 1245 (1998).
- ¹⁴T. Shima, K. Takahashi, Y. K. Takahashi, and K. Hono, *Appl. Phys. Lett.* **81**, 1050 (2002).
- ¹⁵S. Okamoto, O. Kitakami, N. Kikuchi, T. Miyazaki, Y. Shimada, and Y. K. Takahashi, *Phys. Rev. B* **67**, 094422 (2003).
- ¹⁶C. Kuo, P. C. Kuo, and H. Wu, *J. Appl. Phys.* **85**, 2264 (1999).
- ¹⁷P. T. L. Minh, N. P. Thuy, N. D. Van, and N. T. N. Chan, *J. Magn. Magn. Mater.* **239**, 335 (2002).
- ¹⁸Y. Tanaka, N. Kimura, K. Hono, K. Yasuda, and T. Sakurai, *J. Magn. Magn. Mater.* **170**, 289 (1997).
- ¹⁹M. H. Hong, K. Hono, and M. Watanabe, *J. Appl. Phys.* **84**, 4403 (1998).
- ²⁰T. Shima, T. Seki, K. Takahashi, Y. K. Takahashi, and K. Hono, *Proceedings International Conference on Magnetism, Rome, Italy, 2003*.
- ²¹R. C. O'Handley, *Modern Magnetic Materials Principles and Applications* (Wiley-Interscience, New York).
- ²²G. Q. Li, H. Takahashi, H. Ito, H. Saito, S. Ishio, T. Shima, and K. Takahashi, *J. Appl. Phys.* **94**, 5672 (2003).
- ²³S. Okamoto, N. Kikuchi, O. Kitakami, T. Miyazaki, Y. Shimada, and K. Fukamichi, *Phys. Rev. B* **66**, 024413 (2002).